Check for updates

EurJIC
European Journal of Inorganic Chemistry

Research Article
doi.org/10.1002/ejic.202400835

Chemistry Europe
European Chemical Societies Publishing

www.eurjic.org

N,N,N′,N′-Tetrakis((1*H*-Pyrazol-3-Yl)methyl)-1,2-Ethanediamine Ligands as Versatile Scaffolds for Second Coordination Sphere Design

Corentin Pochet,[a] Tristan Laurent,[a] Mengmeng Wang,[a] Aurelian Rotaru,[b] Koen Robeyns,[a] Yann Garcia,[a] and Michael L. Singleton*[a]

The polypyrazole-containing ligands, N,N,N′,N′-tetrakis((5-*tert*-Butyl-1*H*-pyrazol-3-yl)methyl)-1,2-ethanediamine (L1) and N,N,N′,N′-tetrakis((5-Phenyl-1*H*-pyrazol-3-yl)methyl)-1,2-ethanediamine (L2) were synthesized and shown to form hexadentate monometallic coordination compounds with Co^{II}, Ni^{II}, Cu^{II} and Zn^{II} metal ions. Exchange studies with the metal ions show binding preference in the order of $Ni^{II} > Co^{II}/Cu^{II} > Zn^{II}$. The compounds were confirmed by NMR, UV-Vis studies and the X-ray crystals structures of $[Co(L1)](PF_6)_2$, $[Ni(L1)](PF_6)_2$, $[Cu(L1)]ClPF_6$, $[Zn(L1)](PF_6)_2$, and $[Ni(L2)]Cl_2$. In the solid state, the arrangement of the bulky pyrazole units leads to the formation of two distinct cationic pockets containing the N–H groups of the pyrazoles. These cationic pockets are found to bind Cl^- or PF_6^- counterions through hydrogen bonding and anions titrations revealed good affinity for Cl^- and Br^-. The compounds can be dehydronated up to two times using mild organic bases, highlighting the potential of these ligands to tune the electronic properties of the metal center.

Introduction

Second coordination sphere refers to the collection of interactions between a metal complex and its environment. These interactions play a crucial role in the properties and reactivity of coordination compounds and can influence ligand donation,[1] substrate binding,[2] and stability of reactive intermediates.[3] As such, ligands that can harness and specifically orient these interactions offer valuable opportunities to fine-tune chemical properties without directly altering the primary coordination sphere. This has made them important for a range of applications including sensing and catalysis.[4–6] Most commonly, ligand designs rely on the inclusion of hydrogen bonding sites,[7–8] ion pairing,[9] or stimuli-responsive (acidic/basic) groups,[10] with the specific placement of the interactions being dictated by the geometric preferences of the metal and the nature of the ligand scaffold.

In this respect, hexadentate ligands, particularly those containing heterocycles, offer a robust platform for integrating and controlling the placement of second coordination sphere interactions. Typically comprised of ethylene or propylene diamine units functionalized with pendant heterocyclic arms, these structures have found applications in catalysis,[11–13] metal-ion sensing,[14–15] biomedical studies,[16–18] spin-crossover materials,[19] and as general chelating agents for transition metals or lanthanide ions over the last decades.[20–22] As a prototypical example, the TPEN scaffold (Figure 1a) has received significant interest due to its high affinity for a large range of metal ions.[23–29] TPEN transition metal complexes show diverse reactivity, including catalytic water oxidation,[30–31] CO_2 reduction,[32] aromatic hydroxylation,[33] atom transfer radical addition,[34–35] and rapid spin crossover.[36–37] Expanding on this structure, numerous groups have introduced different linkers or heterocyclic moieties into the pendant arms, allowing the tuning of the properties and reactivity of the scaffold and its coordination compounds. Although this has led to a diverse family of ligands, structures containing polyazaheterocyclic units (*e.g.* pyrazoles) in the arms remain rare, and yet the presence of additional free N or N–H groups provides valuable sites for designing interactions between a coordination compound and other chemical species or for further tuning the metal ion properties through external stimuli. Indeed, such

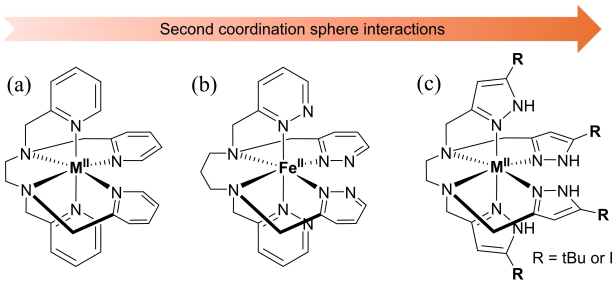


Figure 1. General structures of (a) M^{II} TPEN-based complexes, (b) recent pyridazine-based Fe^{II} coordination compounds,[45] and (c) our M^{II} pyrazolyl-based coordination compounds.

[a] *C. Pochet, T. Laurent, Dr. M. Wang, Dr. K. Robeyns, Prof. Y. Garcia, Prof. M. L. Singleton*
Molecular Chemistry, Materials and Catalysis (MOST), Institute of Condensed Matter and Nanosciences (IMCN), Université catholique de Louvain, 1348 Louvain-la-Neuve, Belgium
E-mail: m.singleton@uclouvain.be

[b] *Prof. A. Rotaru*
Department of Electrical Engineering and Computer Science and MANSiD Research Center, "Stefan cel Mare" University, University Street 13, Suceava 720229, Romania

Supporting information for this article is available on the WWW under https://doi.org/10.1002/ejic.202400835

© 2025 Wiley-VCH GmbH

Research Article
doi.org/10.1002/ejic.202400835

second coordination sphere interactions significantly impact the reactivity and stability of different metal complexes.[38] Recently, our group showed that the additional endocyclic nitrogen atoms in pyridazine-functionalized scaffolds can act cooperatively to bind hydrons (H^+),[39] thereby preventing the decomplexation of Fe^{II} compounds in highly acidic media (Figure 1b). However, pyridazines, and the related electron-deficient polyazaheterocycles, have limited reactivity once coordinated, as the electron-withdrawing effect of the metal ion substantially decreases the nucleophilicity and basicity of the second nitrogen, necessitating strong electrophiles to modify these structures.

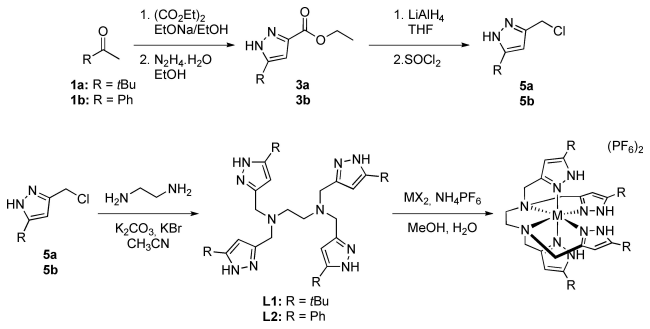
To this end, pyrazoles are particularly attractive for second coordination sphere interactions due to their dual functionality and pyrazole containing ligands have found wide interest in spin crossover materials,[40–41] phosphorescent complexes,[42] and supramolecular chemistry.[43–44] The coordination of the pyridine-like nitrogen atom of the pyrazole to a metal center increases the acidity of the hydron on the pyrrole-like nitrogen and brings several consequences.[45] First, the N–H hydron becomes a better H-bond donor and is able to interact with H-bond acceptors such as anions.[46] The choice of the metal ion and the structure of the pyrazole-containing ligands control the geometry of the coordination compound and the orientation of H-bond donor sites providing directional and specific interactions. Secondly, the increased acidity of the N–H hydrons allows them to be dehydronated under mild conditions which substantially alter metal-based reactivity by increasing the electronic density on the metal center.[5,47–48] Moreover, the dehydronated form of the pyrazole, the pyrazolato anion, can serve as a ditopic bridging ligand by coordinating with another metal centers, making it interesting for the formation of polynuclear complexes,[49–50] supramolecular architectures, coordination polymers and metal-organic frameworks (MOFs).[51]

In this work, we explore the potential of two hexadentate ligands, N,N,N′,N′-tetrakis((5-R-1H-pyrazol-3-yl)methyl)-1,2-ethanediamine [R = *t*-Bu (L1) or Ph (L2)], (Figure 1c) to establish directional second coordination sphere interactions through the strategic placement of pyrazole groups resulting from coordination with Ni^{II}, Co^{II}, Cu^{II}, and Zn^{II}. Structural and spectroscopic studies show the formation of cationic binding sites capable of anion recognition. This is facilitated by the enhanced acidity of the pyrazoles as demonstrated by the dehydronation of the compounds under mild conditions allowing to further tune their reactivity.

Results and Discussion

Synthesis of Ligands and Metal Complexes

The pyrazole-containing ligands, L1 and L2, were synthesized from commercially available *tert*-butyl methyl ketone or acetophenone in five steps, Scheme 1, using a variation of reported procedures.[52–53] After an initial Claisen condensation with diethyl oxalate followed by reaction with hydrazine to give the pyrazole esters, reduction with $LiAlH_4$ and chlorination with



Scheme 1. Synthesis of the ligands and metal complexes starting from the corresponding ketones.

$SOCl_2$ gave the corresponding *tert*-butyl or phenyl-functionalized 3-(chloromethyl)-1H-pyrazoles. These intermediates were subsequently used for the alkylation of 1,2-ethylenediamine in the presence of KBr and K_2CO_3, to afford ligands L1 and L2 in 75% and 55% yield, respectively. This approach ensures the clean incorporation of the pyrazolyl units, allowing easy isolation of the ligands, which precipitate from the solution while the inorganic salts are easily removed by washing with water.

The metal complexes were synthesized by addition of one equivalent of the corresponding hydrated chloride salt to a methanolic solution of the respective ligand. Co compounds synthesis led to dark pink solutions after the coordination of $CoCl_2{\cdot}6H_2O$. Purple solutions were obtained after the addition of the green solid $NiCl_2{\cdot}6H_2O$ to the ligands in solution, whereas the Cu solutions turned to dark blue upon the addition of $CuCl_2{\cdot}2H_2O$ with L1 and to dark green with L2. Colorless solutions were obtained for the Zn compounds. All the coordination compounds can be precipitated from solution as the corresponding colored powders through the addition of solid NH_4PF_6 followed by water. They are highly soluble in polar organic solvents like MeCN, DMSO, alcohols and carbonyls, but only slightly soluble in chlorinated solvents such as $CHCl_3$.

Solid State Structures

Single crystals suitable for X-ray diffraction were obtained for L1Ni, L1Co, L1Zn, and L2Ni by diffusing Et_2O into methanolic solutions of the compounds. All of them crystallize in the monoclinic space group *C2/c* with a twofold axis passing through the equatorial plane (Figures S1–S8), giving 4 molecules in the unit cell ($Z = 4$, $Z' = 0.5$). The individual compounds are chiral but both enantiomers are found in the crystal. Figure 2 shows the structure of one of the two enantiomers. In the Ni, Co and Zn compounds, the ligands coordinate to the metal ions in a hexadentate fashion forming a distorted N_6 octahedral geometry consisting of the two aliphatic amines and four endocyclic nitrogen atom from the four pendant pyrazolyl units, with two pyrazole rings positioned equatorially and two axially. All four compounds possess a *C*2 symmetry axis in the equatorial plane that passes between the pairs of pyrazoles and

© 2025 Wiley-VCH GmbH

10990682c, 2025, 11, Downloaded from https://chemistry-europe.onlinelibrary.wiley.com/doi/10.1002/ejic.202400835 by Universite Catholique De Louvain, Wiley Online Library on [06/06/2025]. See the Terms and Conditions (https://onlinelibrary.wiley.com/terms-and-conditions) on Wiley Online Library for rules of use; OA articles are governed by the applicable Creative Commons License

Research Article
doi.org/10.1002/ejic.202400835

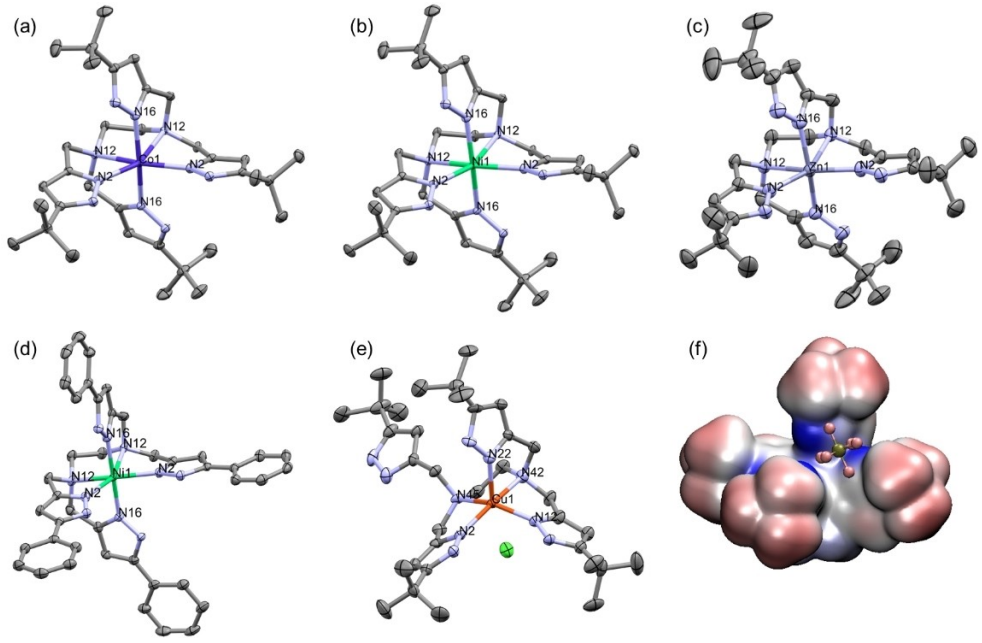


Figure 2. ORTEP representation with displacement ellipsoids drawn at the 50% probability level for (a) L1Co, (b) L1Ni, (c) L1Zn, (d) L2Ni and (e) L1Cu. (f) Calculated electrostatic potential map of L1Ni showing the anion binding pockets in the structure. Hydrogens, solvent molecules, and non-interacting counterions have been omitted for clarity.

aliphatic nitrogen atoms, leading to high symmetry and equivalent bond distances for each pair of nitrogen atoms, (Table 1). The metal-nitrogen bond distances vary between 2.043 and 2.074 Å for L1Ni, 2.083 and 2.243 Å for L1Co, 2.045 and 2.166 Å for L1Zn and between 2.327 and 2.195 Å for L2Ni with the shortest distances being observed for the two axial nitrogen atoms, and the longest for the two "en" nitrogen atoms. The dihedral angle between the two *cis*-equatorial pyrazolyl rings is 22.13° for L1Ni, 20.48° for L1Co, 18.47° for L1Zn, and 14.46° for L2Ni, while the planes of the *trans* pyrazolyl rings are almost perpendicular to one another, with dihedral angles of 85.39° for L1Ni, 83.09° for L1Co, 80.72° for L1Zn, and 81.52° for L2Ni. These values are largely similar to the those of related TPEN complexes, for instance, the dihedral angles between pyridines in $TPENZn(PF_6)_2$ reported by Sadler et al. are 22.5° for the *cis* and 79.9° for the *trans*.[24] Although suitable crystals could not be obtained for all compounds, the infrared spectra of the metal complexes containing the same ligands are highly similar suggesting largely isostructural molecules (Figur-

Table 1. Selected bond lengths (Å) and angles (°) for L1Ni, L1Zn, L1Co, L2Ni, and L1Cu.

Connectivity	L1Ni	L1Zn	L1Co	L2Ni	L1Cu	
M–N(16)	2.0446(13)	2.1144(15)	2.0828(12)	2.045(2)	Cu–N(2)	1.966(4)
M–N(2)	2.0703(13)	2.0741(14)	2.0889(12)	2.114(3)	Cu–N(12)	1.999(5)
M–N(12)	2.1658(12)	2.3265(14)	2.2433(12)	2.195(3)	Cu–N(42)	2.068(5)
					Cu–N(45)	2.081(5)
					Cu–N(22)	2.112(5)
N(16)-M–N(16)	171.84(7)	164.22(9)	168.26(7)	179.36(14)	N(2)-Cu–N(12)	105.47(18)
N(16)-M–N(2)	93.50(5)	95.04(6)	94.33(5)	90.16(10)	N(2)-Cu–N(42)	161.84(19)
N(16)-M–N(2)	90.47(5)	91.42(6)	90.89(5)	90.14(10)	N(12)-Cu–N(42)	80.36(19)
N(2)-M–N(2)	121.67(7)	131.55(8)	127.20(7)	124.76(14)	N(2)-Cu–N(45)	80.80(18)
N(2)-M–N(12)	158.67(5)	151.10(5)	154.73(5)	155.19(10)	N(12)-Cu–N(45)	146.81(19)
N(2)-M–N(12)	78.21(5)	76.28(5)	76.77(5)	78.19(9)	N(42)-Cu–N(45)	85.19(19)
N(16)-M–N(12)	79.90(5)	76.39(5)	78.05(5)	79.58(10)	N(2)-Cu–N(22)	113.18(18)
N(16)-M–N(12)	93.97(5)	91.24(6)	92.96(5)	99.93(10)	N(12)-Cu–N(22)	104.23(19)
N(12)-M–N(12)	83.47(7)	77.88(7)	81.15(6)	81.41(13)	N(42)-Cu–N(22)	81.11(18)
					N(45)-Cu–N(22)	102.80(18)

© 2025 Wiley-VCH GmbH

10990682c, 2025, 11, Downloaded from https://chemistry-europe.onlinelibrary.wiley.com/doi/10.1002/ejic.202400835 by Universite Catholique De Louvain, Wiley Online Library on [06/06/2025]. See the Terms and Conditions (https://onlinelibrary.wiley.com/terms-and-conditions) on Wiley Online Library for rules of use; OA articles are governed by the applicable Creative Commons License

Research Article
doi.org/10.1002/ejic.202400835

es S11 & S12), as seen for the L1 series of coordination compounds in the solid state.

In all the structures, the arrangement of the pyrazole groups leads to two distinct pockets, each generated by two equatorial pyrazoles and one of the axial pyrazoles, flanked by the hydrophobic *t*-Bu or Ph groups. The electrostatic potential map of these pockets, derived from computational studies (*vide infra*), highlights their cationic nature, with the free N–H groups of the pyrazoles, (Figure 2f) representing important binding sites for interaction with other chemical species. Indeed, in the solid state, these pockets contain the PF_6^- (L1Ni, L1Co, and L1Zn) or Cl^- (L2Ni) counterions, which interact through hydrogen bonding with the pyrazole units. In the case of L2Ni, an additional disordered MeOH molecule is also involved in the hydrogen bond network.

Single crystals of X-ray quality were also obtained for L1Cu which crystalizes in the monoclinic space group $P2_1/c$ (Figure 2 and S9–S10). The Cu center is bound in an N_5 coordination environment consisting of the two aliphatic amines and three endocyclic nitrogen atoms from three pyrazolyl units, while the fourth pyrazole ring is present only as a free pendant group. This results in a distorted square-pyramidal geometry, (Addison's parameter $\tau_5 = 0.25$) with N22 as the axial ligand,[54] displaying a longer bond distance (Cu–N22 = 2.112 Å) than the other four nitrogen ligands (1.965–2.079 Å). The compound crystalized with one PF_6^- and one Cl^- ion, which interact in a second-coordination sphere manner through hydrogen bonding with the pyrazolyl NH (NH–Cl distance: 2.229–2.318 Å). As Cu has tendency to undergo Jahn-Teller distortion, the interactions with the Cl^- ion make this effect even more significant, further stabilizing the square pyramidal geometry. The effect of a coordinating anion on Cu[TPEN] complexes has been discussed by Yoon *et al.*[55] and showed that the geometric switch between octahedral and square-pyramidal forms can be controlled by the presence of a Cl^- ion.

NMR/Evans Method Studies

^{1}H NMR spectra in DMSO-d_6 (Figure 3a-b) were recorded for the ligands and their Zn coordination compounds and show downfield shifted signals after metal ion addition. Major shifts are observed for the protons close to the chelating nitrogen atoms,

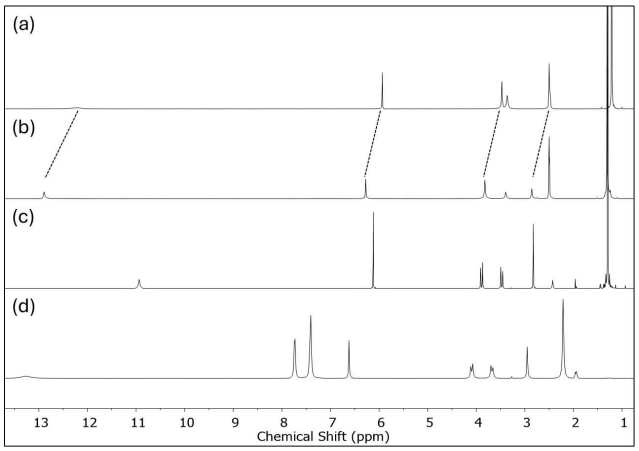


Figure 3. Comparison of the ^{1}H NMR spectra of (a) L1 in DMSO-d_6 (2.50 ppm), L1Zn (b) in DMSO-d_6, (c) in CD_3CN (1.94 ppm) and (d) L2Zn in in CD_3CN.

consistent with Zn complexation as observed for TPEN coordination compounds.[24] In these Zn compounds as well as for the others, octahedral geometry around the metal results in axial chirality, which should lead to the splitting of the methylene resonances into diastereotopic pairs in the NMR spectrum. This effect is absent in DMSO and the CH_2 signal at 3.47 ppm appears relatively broad, suggesting that exchange between the enantiomers is moderately fast compared to the NMR timescale. When the compound is dissolved in less coordinating and less polar solvents, such as acetonitrile, this equilibrium slows down and two clear diastereotopic signals for the pyrazole methylene protons appear at 3.86 and 3.45 ppm for L1Zn, Figure 3c, and at 4.09 and 3.68 ppm for L2Zn, Figure 3d.

All the remaining metal complexes are paramagnetic. The Evans method (Table 2) was used to study their magnetic moment.[56–57] Using the spin-only approximation, the relation between the relative NMR shift, the effective magnetic moment and the number of unpaired electrons was established. The values for the Cu compounds are in relatively good agreement with the expected doublet state for d^9 metal centers. Likewise, the magnetic susceptibility of the Ni compounds indicates the presence of two unpaired electrons due to the octahedral geometry around the metal that favors one electron in each e_g level orbitals. The octahedral Co^{II} compounds are expected to

Table 2. Evans Method analyses, selected UV-Vis analysis values and redox potentials.

Compound	Meas. unpaired electrons[a]	Theo. unpaired electrons	Wavelength/nm (ε/mol^{-1}.L)	E°, V
L1Co	2.65–4.03	3.00 (HS)	998 (5), 492 (40), 465(51)	/
L2Co	2.76–4.11	3.00 (HS)	959 (6), 500(48), 468(47)	0.43
L1Ni	2.05	2.00	930(14), 557(15), 359(21)	1.21
L2Ni	2.35	2.00	916(30), 559(24), 360(65)	1.31
L1Cu	1.17	1.00	687(262), 281(4220)	−0.58
L2Cu	1.33	1.00	668(181)	−0.48

[a] Ni, Cu and Co compounds magnetic susceptibility were measured by Evans method and with SQUID magnetometer for Co compounds. A range of values is expressed for L1- and L2Co going from $L = 3$ to $L = 0$ (For equations, see SI).

© 2025 Wiley-VCH GmbH

10990682c, 2025, 11, Downloaded from https://chemistry-europe.onlinelibrary.wiley.com/doi/10.1002/ejic.202400835 by Universite Catholique De Louvain, Wiley Online Library on [06/06/2025]. See the Terms and Conditions (https://onlinelibrary.wiley.com/terms-and-conditions) on Wiley Online Library for rules of use; OA articles are governed by the applicable Creative Commons License

Research Article
doi.org/10.1002/ejic.202400835

be high-spin (HS) with three unpaired electrons. However, the spin-only approximation for the Evan's method studies with L1Co or L2Co gives four unpaired electrons. As the +2 oxidation state is supported by spectroscopic and X-ray structural studies, as well as chemical reactivity (*vide infra*), the discrepancy between the measured and theoretical values is likely due to unquenched angular momentum, a phenomenon frequently observed in Co^{II} coordination compounds in the literature.[58–60] Including the orbital angular momentum term for determining μ_{eff} and varying *L* from 0 to 3, gives 2.6–4 unpaired electrons, far beyond what would be expected for the low-spin (LS) state suggesting that both Co compounds are high-spin (HS). This was further supported by SQUID measurements (Figure S93) of L1Co, which also suggested a $S = 3/2$ spin-state.

UV/VIS Spectra and Complexation Events

The UV-Vis spectra for the compounds were recorded in MeCN and important transitions are summarized in Table 2. Below 250 nm, all the coordination compounds behave the same, showing one absorption band at $\lambda = 220$ nm. Based on the low wavelengths and high molar absorptivity values, these bands are attributed to π–π^* transitions within the ligands, specifically in the pyrazolyl rings. Otherwise, the Ni compounds behavior aligns with previous reported pyrazole-based complexes.[61] The octahedral geometry with its high symmetry around the Ni^{II} ion tends to trigger three low-intensity metal-based transitions, which appear at $\lambda = 930$, 557, and 359 nm for L1Ni and 916, 559, and 360 nm for L2Ni. The broad *d-d* transitions for the Cu compounds are also similar to most penta- or hexa-coordinated Cu complexes in the literature.[62] L1Cu also exhibits a ligand to metal-charge (LMCT) transition at $\lambda = 281$ nm. Two close *d-d* transitions are observed between 460–500 nm and a third broad *d-d* transition is observed above 950 nm for the Co compounds consistent with other HS Co^{II} complexes.[63]

While the transitions are largely similar for each metal, the nature of the substituents on the ligand has a stronger influence on the absorptions at shorter wavelengths. Indeed, for the L2 series, a second absorption band attributed to the phenyl group appears below 300 nm with higher molar absorptivity. This new π–π^* transition hides the MLCT of L2Cu where it is exhibited in L1Cu. Another consequence of substituents is their impact on the observed *d-d* bands. *Tert*-butyl groups being stronger σ-donors and Ph-groups better π-acceptors, the *d-d* band of L2Ni are displaced to higher energies. This hypsochromic shift is also observed in the Co and Cu compounds. The molar absorptivity of the lowest wavelength *d-d* bands for the L2Ni was also observed to increase but this rather comes from the overlapping with the larger π–π^* transitions of ligands.

In agreement with the stoichiometry observed in the X-ray structures, Job's plot experiments (by NMR for Zn or UV-Vis for Cu, Ni and Co) in solution for each coordination compound (Figures S11–S18) confirm the 1:1 ligand to metal stoichiometry, indicating that the monometallic entity is the major species. The shape of UV-Vis spectral variations indicates a strong affinity between the metal ions and the ligands as observed for hexadentate coordination sites.[64] This strong affinity is more highlighted by NMR experiments for L1Zn and L2Zn, as the Zn compounds and the free ligands are in slow exchange on the NMR time scale and the maximum formation is observed with 1:1 stoichiometry.

Electrochemical Behavior

Cyclic voltammograms were recorded in the potential range −2 V to 1.5 V *vs* $Ag/AgNO_3$ in MeCN (0.1 M $TBA(PF_6)$ as the supporting electrolyte), at scan rate of 100 mVs^{-1}, with ferrocene (Fc) (0,087 mV *vs* $Ag/AgNO_3$ 0.01 M) used as an internal standard. [65] The voltammograms of the Cu compounds (Figure 4a) each show a reversible redox event attributed to the Cu^{II}/Cu^{I} couple at −0.65 V and −0.48 V vs Fc^+/Fc for L1Cu and L2Cu, respectively. No ligand reduction was observed, however, the shoulder on the anodic wave in L1Cu indicates the presence of the Cu^{I}/Cu^{0} couple.[66] As no free Cu was observed by UV and the shouldering was absent with a shorter potential window (Figures S20 & S26), we suspected partial release of Cu due to the ligand degradation upon reduction. A similar effect is seen with the ligand reduction in

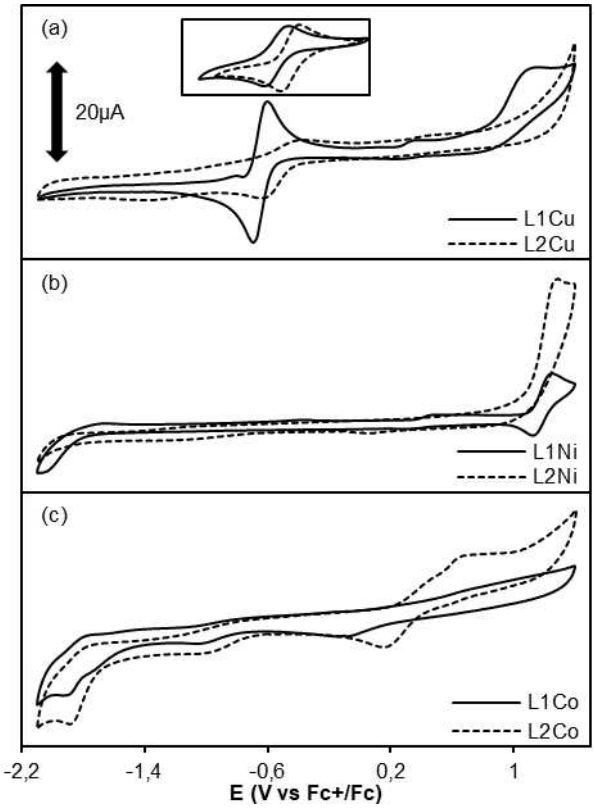


Figure 4. Cyclic voltammograms L1 (solid line) and L2 coordination compounds (dash line) at 100 mV/s in CH_3CN. Concentration : 1 mM. Inset: Cyclic voltammograms of L1Cu and L2Cu in shorter window showing the reversibility of the redox process.

© 2025 Wiley-VCH GmbH

10990682c, 2025, 11, Downloaded from https://chemistry-europe.onlinelibrary.wiley.com/doi/10.1002/ejic.202400835 by Universite Catholique De Louvain, Wiley Online Library on [06/06/2025]. See the Terms and Conditions (https://onlinelibrary.wiley.com/terms-and-conditions) on Wiley Online Library for rules of use; OA articles are governed by the applicable Creative Commons License

Research Article
doi.org/10.1002/ejic.202400835

L2Cu impacting the reversibility of the metal-based redox process.

For the Ni compounds, a reversible oxidation to Ni^{III} was observed at 1.21 V *vs* Fc^+/Fc in L1Ni (Figure 4b). In L2Ni, an irreversible oxidation wave to Ni^{III} occurs at 1.31 V vs Fc^+/Fc with the current showing a more than 2-fold increase in intensity relative to L1Ni. For comparison, this oxidation occurs at higher potential than in TPEN–Ni which undergoes a quasi-reversible oxidation at 1.18 V *vs* Fc^+/Fc.[28] Replacing the pyridine moiety in the TPEN scaffold by phenyl-pyrazole suggests weaker electron-donation from the pyrazole, leading to a less electron-rich Ni center. In contrast, no CV wave indicated the existence of $[L1Ni]^+$ whereas the reduction to $[TPENNi]^+$ occurs at −1.88 V *vs* Fc^+/Fc.[28]

In the case of L1- or L2Co, the voltammograms show multiple and more complex reduction and oxidation events (Figure 4c). The irreversible reduction events at −1.88 V and −1.86 V are tentatively assigned to ligand-centered reductions. The CV waves at positive potential are more likely metal-centered, corresponding to the Co^{III}/Co^{II} couple based on reported data and are less resolved,[30,67] with large peak-to-peak separations and/or irreversibility. Such electrochemical behavior has been previously observed and is likely due to a slow electron self-exchange rate between the Co^{II} and Co^{III} centers at the electrode surface, in comparison to the electron transfer rate between the electrode and the Co ions.[68] This redox process might also be coupled to a spin state switch that increases the energy needed to go back to Co^{II} HS species.[69]

As also suggested by the UV analyses, the presence of the Ph or *t*-Bu units has a moderate effect on the electrochemical properties of the compounds. Given the similar structure of the ligands, the positive shift for the redox potentials for L2 series is most likely due to the electron-withdrawing effect of the Ph substituents. Indeed, the overall change is consistent with the metal centers being less electron rich in these coordination compounds.

Metal Exchange

Based on the similar structures, exchange studies were performed to assess the relative affinity of the ligands for the different metals. Each compound was dissolved in CH_3CN with one equivalent of another metal chloride at 20 °C, and the UV spectra of the resulting mixtures were recorded over several hours (Figures S31–S48).

For the Zn compounds, the addition of Ni, Cu or Co chloride induces immediately the formation of the corresponding Ni, Cu or Co coordination compounds. The exchange is supported by the disappearance of the signals corresponding to the free cations in solution and the apparition of the *d-d* transition of the coordination compounds. The Ni, Cu or Co compounds were also mixed with $ZnCl_2$, and their *d-d* transition stayed unchanged over an extended period of time supporting that the Zn cations are the most labile.

Observing the exchange between Cu and Ni is complicated by the low absorption of the Ni compounds and the larger absorption of free Cu which covers the signals. Still, adding one equivalent of $NiCl_2{\cdot}6H_2O$ to a solution of L1Cu leads to the immediate appearance of free Cu suggesting fast replacement by Ni and more stable complex formation. Similar changes were observed when one equivalent of $CuCl_2{\cdot}2H_2O$ was added to a solution L1Ni or when the L2 compounds were used. In all cases, the specific absorbance of the free Cu at $\lambda = 466$ nm is still present and no *d-d* transitions corresponding to the Cu compounds were detected. However, while no coordination of the Cu could be observed, the absorption for the free Cu slowly decreases over 3 h. The difference in absorption represents an ~20% decrease in the amount of the free Cu. This may be due to interaction with the formed Ni compound, though any other species, if formed, could not be identified.

Exchange between Co and Ni also favors the Ni compounds. Starting from L1- or L2Co, the progressive addition of Ni^{II} results in the appearance of the signal of free Co^{II}, indicating its release during the experiments. In the other way, starting with L1- or L2Ni, no substantial change was observed for the characteristic transition of free Co^{II}.

Relative to the more direct exchange observed in the other systems, large deviations were observed when L1- or L2Cu or L1- or L2Co were mixed with the mixed with, respectively, Co^{II} or Cu^{II} salts (Figure 5). Notably, a new absorption band started to appear at $\lambda = 520$ nm for the L1 systems. A similar behavior was observed for L2, where the overall absorption increased dramatically. The characteristic Cu transition at $\lambda = 466$ nm was not visible, indicating the consumption of the Cu salt and the transition of the Co salt at $\lambda = 680$ nm increased suggesting the presence of free Co^{II} in solution. However, the resulting spectrum could not fit any mixture of the corresponding coordination compounds or free salts (Figures S13 & S14). Instead, a mix of free Co^{II} and a new species absorbing around $\lambda = 500$ nm is observed. This absorption is consistent with Co^{III} complexes in a N_6 environment (vide infra),[63] suggesting potential redox events occurring during the metal exchange. Still, this is not quantitative and substantial free Co^{II} remains in solution, so the formation of more complex multimetallic or polymeric structures cannot be ruled out.

Based on the exchange studies, the stability of the coordination compounds with L1 and L2 follows the order Ni > Co/Cu > Zn. The reactivity observed with Co and Cu makes

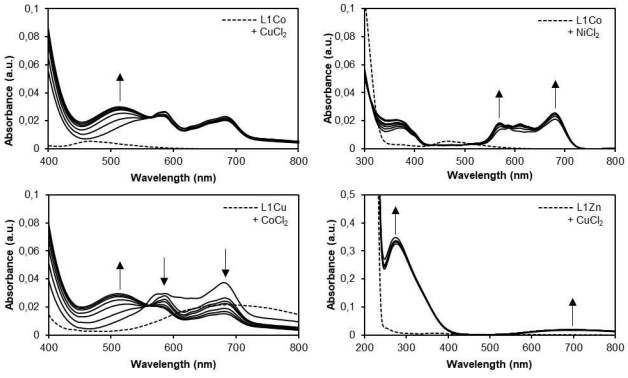


Figure 5. UV-Vis spectra of the mixing experiments in CH_3CN.

© 2025 Wiley-VCH GmbH

10990682c, 2025, 11, Downloaded from https://chemistry-europe.onlinelibrary.wiley.com/doi/10.1002/ejic.202400835 by Universite Catholique De Louvain, Wiley Online Library on [06/06/2025]. See the Terms and Conditions (https://onlinelibrary.wiley.com/terms-and-conditions) on Wiley Online Library for rules of use; OA articles are governed by the applicable Creative Commons License

Research Article
doi.org/10.1002/ejic.202400835

determination of their relative stabilities difficult. However, the slower rate of exchange with Ni suggests that the Co compounds are potentially slightly more stable than the Cu compounds. This is likely due to the non-coordinated pendant pyrazole group in L1- or L2Cu, which can help to bind to a second metal. Notably, the stability of Cu structures does not obey the Irving-Williams series for first row M^{II} transition metal ions, which can be attributed to its five-coordinate structure compared to octahedral coordination for the other M^{II} first-row transition-metal complexes.[24]

Dehydronation Reactivity

The specificity of the pyrazoles, compared to pyridine or pyridazine, for instance, is their ability to reach different hydronation states, opening the possibility of fine-tuning of the properties of the coordinated metal. This was illustrated for the electrochemical properties for Ru complexes by Sullivan.[70] As the L1 and L2 coordination compounds possess four accessible hydrons, one on each pyrazolyl ring, dehydronation offers access to multiple different states, making this reactivity interesting to study.

To this end, the dehydronation was followed by UV and NMR (Figures S49-S64) using DBU (1,8-diazabicyclo[5.4.0]undec-7-ene) as the base. The Cu compounds undergo a hypsochromic shift with slight diminution of the molar absorptivity upon the first dehydronation. Then, a progressive second dehydronation occurs for L1Cu (Figure 6) indicated by the appearance of a new *d-d* band at $\lambda = 643$ nm while it takes two equivalents of base to observe the same pattern on L2Cu accompanied by its precipitation, supported by the overall increase in absorbance.

By contrast, the Ni compounds first undergo a hyperchromic shift upon their first dehydronation, followed by a bathochromic shift upon the second dehydronation going from 558 to 563 nm for L1Ni and from 560 to 590 nm for L2Ni. This behavior is consistent with the metal being more electron-rich due to the increased electronic density on the ligand.

Dehydronation of the Zn compounds, monitored by NMR, leads to the coalescence of the methylene protons and induces an upfield shift for all the protons except the methylenes of the ethane moiety. However, the increase of DBU equivalents progressively broadened all the signals for L1Zn complicating further analysis. A similar broadening of signals was observed for L2Zn due to the precipitation of the mono-dehydronated species, which is resolubilized after the addition of a second equivalent of DBU, leading again to sharp signals. Based on these observations, the formation of neutral compounds seems to drive the dehydronation, but the pKa of the third and the fourth hydrons makes them inaccessible under these conditions. Of note, when a weaker base such as triethylamine (TEA) is used, even in large excess, it has the same effect as one equivalent of DBU for all coordination compounds showing that TEA does not access the second dehydronation. In all cases, the behavior observed by dehydronation is reversible. The addition of trifluoroacetic acid restores the spectra of the hydronated species.

Although X-ray quality crystals could not be obtained for the dehydronated species, theoretical studies (b3lyp//lanl2dz /D95) on L1Ni were used to give insight into the structures generated by the first and second dehydronations (Figure 7). Given the octahedral structures, loss of the first hydron can occur on either an equatorial or axial pyrazole, with the calculations suggesting equatorial dehydronation should be favored by 3.4 kcal/mol and appears to result from potential stabilization of the anionic N by the electropositive N–H of the second equatorial pyrazole. For the second dehydronation four different combinations are possible: equatorial/equatorial; axial/axial; or two different combinations of equatorial/axial where the axial pyrazole is connected to either the same linker nitrogen or the opposite linker nitrogen. In this case, the equatorial dehydronation is again predicted, with the equatorial/equatorial isomer favoured by ~2 kcal/mol versus the other doubly dehydronated isomers and slightly more favoured (0.24 kcal/mol relative to the most stable monodehydronated

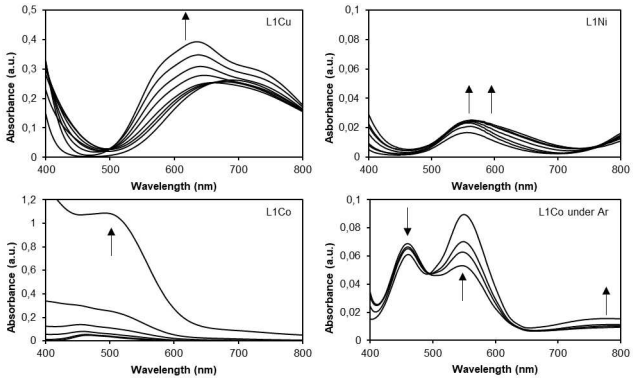


Figure 6. UV-Vis spectra of the titration of L1Cu and L1Ni from 0–10 equiv. of DBU in CH_3CN, L1Co from 0–2 equiv. and L1Co from 1–2 equiv. under Ar.

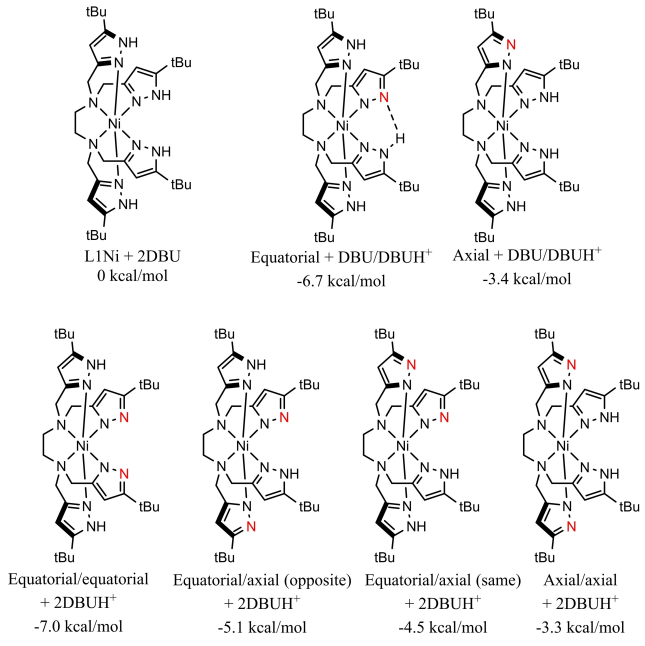


Figure 7. Dehydronation possibilities of L1Ni and their relative energies.

© 2025 Wiley-VCH GmbH

10990682c, 2025, 11, Downloaded from https://chemistry-europe.onlinelibrary.wiley.com/doi/10.1002/ejic.202400835 by Universite Catholique De Louvain, Wiley Online Library on [06/06/2025]. See the Terms and Conditions (https://onlinelibrary.wiley.com/terms-and-conditions) on Wiley Online Library for rules of use; OA articles are governed by the applicable Creative Commons License

Research Article
doi.org/10.1002/ejic.202400835

structure). Products resulting from three or four dehydronations were only found to be higher in energy than the starting L1Ni.

In contrast to the Ni or Cu compounds, L1Co (Figure 7) and L2Co (Figures S59 & S60) displayed more complex behavior upon dehydronation. One equivalent of DBU led to an increase of the absorption of the *d-d* transition consistent with the observations for the Ni compounds. Upon addition of the second equivalent, three new transitions were identified at $\lambda =$ 784, 556 and 463 nm for L1Co and two at $\lambda = 562$ and 461 nm for L2Co. Evan's method analysis of L1Co with DBU showed a substantial decrease in μ_{eff}, values, but still suggests 3 unpaired electrons. However, the dehydronation of L1Co or L2Co must be performed under an inert atmosphere. In the presence of O_2, the addition of a second equivalent of DBU led a strong increase in the absorbance below 350 nm associated to a charge transfer and a new absorption band at $\lambda = 500$ nm with moderate molar absorptivity, consistent with structurally related Co^{III} complexes,[63] suggesting oxidation. Further support for the oxidation came from comparison with the chemically oxidized species, synthesized by adding one equivalent of CAN (cerium ammonium nitrate), a one electron oxidant, to a solution containing Co^{II} compounds. UV-Vis analysis after oxidation shows the same absorption band around 500 nm and the charge transfer at $\lambda = 345$ nm. Moreover, the NMR spectrum after dehydronation and oxidation was recorded showing a diamagnetic species associated to the LS Co^{III} coordination compound, with clear splitting of the signals for the axial and equatorial pyrazoles (Figure S58).

Anion Recognition

Given the increased acidity of the pyrazole hydrons and the close contacts between L2Ni and chloride in the solid state, the potential for the compounds to interact with halides in a second-coordination-sphere manner was investigated. Anion titrations, by UV spectroscopy, were performed in CH_3CN using $(n\text{-Bu})_4NCl$ or $(n\text{-Bu})_4NBr$. L1Ni and L1Co were chosen for this study as these compounds could be isolated with only PF_6^- ions, avoiding competition with already present halide ions.

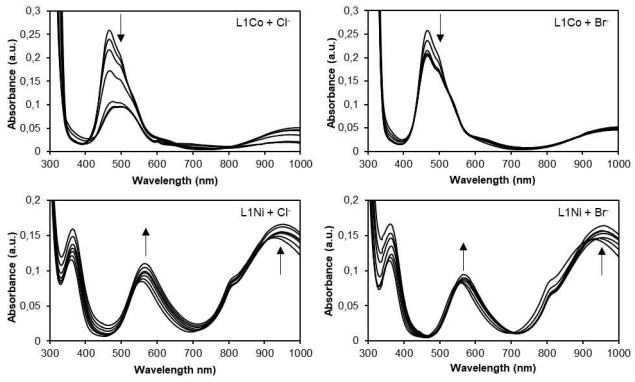


Figure 8. UV spectra of the titration of L1Co and L1Ni from 0–8 equiv. of $(n\text{-Bu})_4NCl$ and $(n\text{-Bu})_4NBr$ in CH_3CN.

The addition of either bromide or chloride to L1Ni (Figure 8) result in similar spectral changes, with bathochromic shifts of the *d-d* transitions, similar to what is observed during the dehydronation experiments. Continued addition leads to an increase in the absorbance for these bands. Using Bindfit,[71–72] a 1:2 binding model was found to give the best fit with $K_{1:1} = 183 \pm 79$ and $K_{1:2} = 17 \pm 8$ for chloride and $K_{1:1} = 6438 \pm 194$ and $K_{1:2} = 55 \pm 8$ for bromide.

In contrast to the Ni compound, the addition of chloride to L1Co causes a substantial decrease of molar absorptivity at the *d-d* transitions and changes the shape of UV absorption signals (Figure 8) with the lowest energetic transition shifting from 998 nm to 968 nm and the two transitions at 492 and 465 nm shifting to 503 and 482 nm, respectively. Similar to the L1Ni experiments, a 1:2 binding was found with $K_{1:1} = 331 \pm 24$ and $K_{1:2} = 34 \pm 18$. With up to one equivalent of bromide the decrease of molar absorptivity at 465 nm for L1Co (Figure 8) is identical to what is observed with chloride. However, with subsequent aliquots of bromide, no further significant decrease is observed. Fitting of the data in this case gives only a 1:1 binding with $K_{1:1}$ (L1Co/Br) $= 6094 \pm 493$, similar to the first binding event observed between L1Ni and bromide.

Globally, the similar behavior observed for chloride or bromide with each coordination compound suggests a similar mode of interaction, with the higher association of bromide likely being primarily due to its lower desolvation energy.[73] The lower association constant for the second binding event with the anions is consistent with ion-ion interactions being the main driving force for binding of the halides and the negative cooperativity observed. Still, the spectral changes are similar, though smaller in magnitude, to what was observed during the dehydronation experiments. This can be expected as hydrogen bonding should also lead to increased electron density on the pyrazole units. Based on the crystal structure for L2Ni, it is likely that in the 1:2 complex the two anions would be bound in the two cationic pockets. Whether pocket binding would also be preferred for the 1:1 complex is less evident. Based on the higher calculated acidities of the equatorial pyrazoles and the convergent arrangement of their N–H groups, the initial binding could rather involve only these units acting to chelate the anions. DFT studies looking at the anion binding found that, while indeed the lowest energy structure for the 1:2 complex had the halides in the cationic pockets, all attempts to place the anion in a pocket for the 1:1 complex converged to an equatorial-equatorial chelating structure, Figure 9.

Conclusions

In summary, two N_6 hexadentate ligands bearing pyrazole groups were synthesized and their coordination with 3d transition metals was investigated. The resulting polypyrazolyl mononuclear metal coordination compounds were characterized by NMR, UV-Vis, IR, by X-ray diffraction and electrochemical methods. Both solution and solid-state studies indicate that the ligands lead to similar octahedral structures, with the exception of the Cu compounds, which adopt a distorted square

© 2025 Wiley-VCH GmbH

10990682c, 2025, 11, Downloaded from https://chemistry-europe.onlinelibrary.wiley.com/doi/10.1002/ejic.202400835 by Universite Catholique De Louvain, Wiley Online Library on [06/06/2025]. See the Terms and Conditions (https://onlinelibrary.wiley.com/terms-and-conditions) on Wiley Online Library for rules of use; OA articles are governed by the applicable Creative Commons License

Research Article
doi.org/10.1002/ejic.202400835

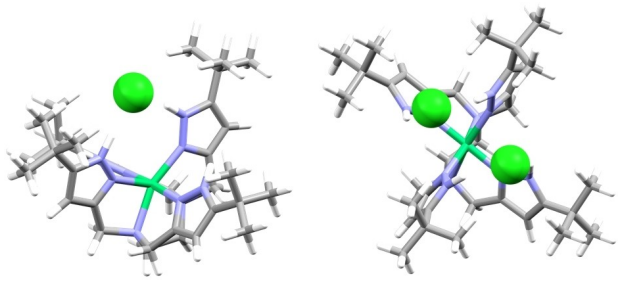


Figure 9. DFT optimized structures for the 1:1 (left) and 1:2 (right) complexes formed from L1Ni and Cl^-.

pyramidal geometry. Stability assessments from exchange studies indicate the order of stability as Ni > Co/Cu > Zn. Across the series, the substituents on the pyrazole (*t*-Bu *vs* Ph) have only modest effects on the spectroscopic and electrochemical properties of the metal but do impact the solubility during dehydronation.

The hexadentate nature of the ligands precisely positions the pyrazole N–H groups, providing a versatile scaffold for second coordination sphere interactions. The reactivity of L1Co and L2Co already highlight the potential to use second coordination sphere modifications to enable bifunctional activation via a dehydronation-oxidation process with oxygen. More generally, as we have shown, the hydronated form of the compounds offers cationic sites suitable for interaction with anions. With the observed dehydronation or by further modification of the scaffold, the properties of the compounds could be tuned to provide more specific interactions with different chemical species. As an example, after dehydronation, the new nature of the compounds could favor interactions with cations instead of anions and could represent interesting ligands for the formation of more complex multimetallic structures.

Supporting Information Summary

Further synthetic descriptions, IR, UV-vis, and NMR spectral data are provided in the Supporting Information. CCDC deposition numbers 2410022 (for L1Co), 2410023 (for L2Ni), 2410024 (for L1Zn), 2410025 (for L1Ni), and 2410026 (for L1Cu) contain the supplementary crystallographic data for this paper. The data can be obtained free of charge from The Cambridge Crystallographic Data Centre via www.ccdc.cam.ac.uk/structures. The authors have cited additional references within the Supporting Information.[74–83]

Acknowledgements

We thank the Université catholique de Louvain for financial support. C.P. was supported through a doctoral fellowship from the Belgian National Fund for Scientific Research (FNRS-FRIA). Fonds de la Recherche Scientifique-FNRS (PDR T.0095.21, FC 53249). Computational resources have been provided by the supercomputing facilities of the Université catholique de Louvain (CISM/UCL) and the Consortium des équipements de Calcul Intensif en Fédération Wallonie Bruxelles (CPCI) funded by the Fonds de la Recherche Scientifique – FNRS under convention 2.5020.11. We also thank Fabio Luccacioni for the elemental analyses, Laurent Collard for the MS analyses, and Dr. Gabriella Barozzino for help with the Evan's method analysis of the compounds.

Conflict of Interests

The authors declare no conflict of interest.

Data Availability Statement

The data that support the findings of this study are available in the supplementary material of this article.

Keywords: Pyrazoles · Second Coordination Sphere · Dehydronation · Anion Interactions

[1] A. L. Robinson, E. Bannerman, R. Guillot, C. Herrero, K. Sénéchal-David, E. Rivière, F. Banse, J.-N. Rebilly, *Eur. J. Inorg. Chem.* **2024**, *27*, e202300694.
[2] T. J. Schmeier, G. E. Dobereiner, R. H. Crabtree, N. Hazari, *J. Am. Chem. Soc.* **2011**, *133* (24), 9274–9277.
[3] R. L. Shook, A. S. Borovik, *Inorg. Chem.* **2010**, *49* (8), 3646–3660.
[4] S. Shinoda, *Chem. Soc. Rev.* **2013**, *42*, 1825–1835.
[5] M. A. Halcrow, *New J. Chem.* **2014**, *38*, 1868–1882.
[6] D. Z. Zee, M. Nippe, A. E. King, C. J. Chang, J. R. Long, *Inorg. Chem.* **2020**, *59* (7), 5206–5217.
[7] C.-C. G. Yeh, T. Mokkawes, J. M. Bradley, N. E. Le Brun, S. P. de Visser, *ChemBioChem* **2022**, *23*, e202200257.
[8] S. Amanullah, P. Gotico, M. Sircoglou, W. Leibl, M. J. Llansola-Portoles, T. Tibiletti, A. Quaranta, Z. Halime, A. Aukauloo, *Angew. Chem. Int. Ed.* **2024**, *63*, e202314439.
[9] S. P. de Visser, *Chem. Eur. J.* **2020**, *26*, 5308–5327.
[10] P. Msellem, M. Dekthiarenko, N. H. Seyd, G. Vives, *Beilstein J. Org. Chem.* **2024**, *20*, 504–539.
[11] I. Bernal, I. M. Jensen, K. B. Jensen, C. J. McKenzie, H. Toftlund, J.-P. Tuchagues, *J. Chem. Soc. Dalton Trans.* **1995**, *22*, 3667–3675.
[12] V. Balland, F. Banse, E. Anxolabéhère-Mallart, M. Nierlich, J.-J. Girerd, *Eur. J. Inorg. Chem.* **2003**, *13*, 2529–2535.
[13] K. Sénéchal-David, C. Buron, N. Ségaud, J.-N. Rebilly, A. Dos Santos, J. Farjon, R. Guillot, C. Herrero, T. Inceoglu, F. Banse, *Chem. Eur. J.* **2019**, *25*, 12405–12411.
[14] Y. Mikata, S. Takeuchi, E. Higuchi, A. Ochi, H. Konno, K. Yanai, S. Sato, *Dalton Trans.* **2014**, *43*, 16377.
[15] Y. Mikata, K. Nozaki, M. Tanaka, H. Konno, A. Matsumoto, M. Kawamura, S. Sato, *Inorg. Chem.* **2020**, *59*, 5313–5324.
[16] L. Valencia, P. Pérez-Lourido, R. Bastida, A. Macias, *Cryst. Growth Des.* **2008**, *8* (7), 2080–2082.
[17] D. Lakk-Bogath, N. P. Juraj, B. I. Meena, B. Peric, S. I. Kirin, J. Kaizer, *Molecules* **2021**, *26*, 3220.
[18] F. Mei, C. Ou, L. Cao, F. Hang, X. Meng, J. Li, D. Li, Z. Liao, *Dalton Trans.* **2010**, *39*, 4267–4269.
[19] J. K. McCusker, H. Toftlund, A. L. Rheingold, D. N. Hendrickson, *J. Am. Chem. Soc.* **1993**, *115* (5), 1797–1804.
[20] J. B. Mandel, B. E. Douglas, *Inorg. Chem. Acta* **1989**, *155*, 55–69.
[21] L. Southcott, X. Wang, N. Choudhary, L. Wharton, B. O. Patrick, H. Yang, K. Zarschler, M. Kubeil, H. Stephan, M. Jaraquemada-Pelaez, C. Orvig, *Inorg. Chem.* **2021**, *60* (16), 12186–12196.
[22] R. Ferreiros-Martinez, D. Esteban-Gomez, C. Platas-Iglesias, A. de Blas, T. Rodriguez-Blas, *Inorg. Chem.* **2009**, *48* (23), 10976–10987.

© 2025 Wiley-VCH GmbH

10990682c, 2025, 11, Downloaded from https://chemistry-europe.onlinelibrary.wiley.com/doi/10.1002/ejic.202400835 by Universite Catholique De Louvain, Wiley Online Library on [06/06/2025]. See the Terms and Conditions (https://onlinelibrary.wiley.com/terms-and-conditions) on Wiley Online Library for rules of use; OA articles are governed by the applicable Creative Commons License

[23] G. Anderegg, F. Wenk, *Helv. Chim. Acta* **1967**, *50*, 2330–2332.
[24] C. A. Blindauer, M. T. Razi, S. Parsons, P. J. Sadler, *Polyhedron* **2006**, *25*, 513–520.
[25] C. Hureau, S. Blanchard, M. Nierlich, G. Blain, E. Rivière, J.-J. Girerd, E. Anxolabéhère-Mallart, G. Blondin, *Inorg. Chem.* **2004**, *43* (14), 4415–4426.
[26] S. Groni, C. Hureau, R. Guillot, G. Blondin, G. Blain, E. Anxolabéhère-Mallart, *Inorg. Chem.* **2008**, *47* (24), 11783–11797.
[27] J. Eriksen, P. Goodson, A. Hazell, D. J. Hodgson, K. Michelsen, O. Monsted, J. C. Rasmussen, H. Toftlund, *Acta Chem. Scand.* **1999**, *53*, 1083–1092.
[28] D. Da Luz, C. V. Franco, I. Vencato, A. Neves, Y. Primerano Mascarenhas, *J. Coord. Chem.* **1992**, *26*, 269–283.
[29] L. Duelund, R. Hazell, C. J. McKenzie, L. P. Nielsen, H. Toftlund, *J. Chem. Soc. Dalton Trans.* **2001**, *22*, 152–156.
[30] Q. Xie, Q. Fu, H.-B. Cui, B.-H. Luo, W.-Q. Liu, R. Qiao, Y.-J. Ren, F. Chen, H.-X. Zhang, J.-Q. Long, *Polyhedron* **2020**, *189*, 114731, ISSN 0277–5387.
[31] Q. J. Li, Y.-J. Ren, Q. Xie, M. Wu, H.-X. Feng, L.-M. Zheng, H. X. Zhang, J.-Q. Long, T.-S. Wang, *Appl. Organomet. Chem.* **2020**, *34*, e5813.
[32] L. E. Lieske, A. L. Rheingold, C. W. Machan, *Sustain. Energy Fuels* **2018**, *2*, 1269–1277.
[33] A. Thibon, J.-F. Bartoli, R. Guillot, J. Sainton, M. Martinho, D. Mansuy, F. Banse, *J. Mol. Catal.* **2008**, *287*, 115–120.
[34] A. Kaur, E. E. Gorse, T. G. Ribelli, C. C. Jerman, T. Pintauer, *Polymer* **2015**, *72*, 246–252.
[35] H. Tang, N. Arulsamy, M. Radosz, Y. Shen, N. V. Tsarevsky, W. A. Braunecker, W. Tang, K. Matyjaszewski, *J. Am. Chem. Soc.* **2006**, *128* (50), 16277–16285.
[36] H.-R. Chang, J. K. McCusker, H. Toflund, S. R. Wilson, A. X. Trautwein, H. Winkler, D. N. Hendrickson, *J. Am. Chem. Soc.* **1990**, *112*, 6814–6827.
[37] G. Chen, G. Espinoza-Perez, A. Zentella-Dehesa, I. Silaghi-Dumitrescu, F. Lara-Ochoa, *Inorg. Chem.* **2000**, *39*, 3440–3448.
[38] W. A. Hoffert, M. T. Mock, A. M. Appel and J. Y. Yang, *Eur. J. Inorg. Chem.* **2013**, *22*, 3846–3857.
[39] A. Hammoud, J.-B. Nshimyumuremyi, J. Bourotte, F. Lucaccioni, K. Robeyns, M. M. Dirtu, Y. Garcia, M. L. Singleton, *Eur. J. Inorg. Chem.* **2018**, *27*, 3253–3263.
[40] C.-W. Lu, Y. Wang, Y. Chi, *Chem. Eur. J.* **2016**, *22*, 17892–17908.
[41] J. Olguin, S. Brooker, *Coord. Chem. Rev.* **2011**, *255*, 203–240.
[42] T.-Y. Li, J. Wu, Z.-G. Wu, Y.-X. Zheng, J.-L. Zuo, Y. Pan, *Coord. Chem. Rev.* **2018**, *374*, 55–92.
[43] J. Pérez, L. Riera, *Eur. J. Inorg. Chem.* **2009**, *33*, 4913–4925.
[44] J. Pérez, L. Riera, *Chem. Commun.* **2008**, *44*, 533–543.
[45] J. Pérez, L. Riera, *Chem. Soc. Rev.* **2008**, *37*, 2658–2667.
[46] J. Reedijk, *Recl. Trav. Chim. Pays-Bas* **1969**, *88*, 1451–1470.
[47] S. Trofimenko, *Chem. Rev.* **1972**, *72*, 497–509.
[48] W.-S. Lin, S. Kuwata, *Molecules* **2023**, *28*, 3529.
[49] M. Viciano-Chumillas, S. Tanase, L. J. de Jongh, J. Reedijk, *Eur. J. Inorg. Chem.* **2010**, *22*, 3403–3418.
[50] A. L. Gavrilova, B. Bosnich, *Chem. Rev.* **2004**, *104*, 349–383.
[51] T. Baishya, R. M. Gomila, M. Barcelo-Oliver, D. M. Gil, M. K. Bhattacharyya, A. Frontera, *Crystals* **2023**, *13*, 203.
[52] A. Tanaka, T. Terasawa, H. Higahara, Y. Sakuma, N. Ishibe, M. Sawada, H. Takasugi, H. Tanaka, *J. Med. Chem.* **1998**, *41* (13), 2390–2410.
[53] I. D. Alshakova, I. Korobkov, L. G. Kuzmina, G. I. Nikonov, *J. Org. Chem.* **2017**, *853*, 68–73.
[54] A. W. Addison, N. T. Rao, J. Reedijk, J. van Rijn, G. C. Verschoor, *J. Chem. Soc. Dalton Trans.* **1984**, *7*, 1349–1356.
[55] D. C. Yoon, C. E. Oh, *Bull. Korean Chem. Soc.* **2004**, *25*, 796–800.
[56] K. De Buysser, G. G. Herman, E. Brunel, S. Hoste, I. Van Driessche, *Chem. Phys.* **2005**, *315*, 286–292.
[57] G. A. Bain, J. F. Berry, *J. Chem. Educ.* **2008**, *85*, 532–536.
[58] G. K. Gransbury, M.-E. Boulon, R. A. Mole, R. W. Gable, B. Moubaraki, K. S. Murray, L. Sorace, A. Soncini, C. Boskovic, *Chem. Sci.* **2019**, *10*, 8855–8871.
[59] A. M. Bryan, W. A. Merrill, W. M. Reiff, J. C. Fettinger, P. P. Power, *Inorg. Chem.* **2012**, *51*, 3366–3373.
[60] M. J. Bagley, D. Nicholls, B. A. Warburton, *J. Chem. Soc. A, Inorg. Phys. Chem.* **1970**, *0*, 2694–2697.
[61] M. Di Vaira, F. Mani, P. Stoppioni, *Dalton Trans.* **1994**, *1*, 3739–3743.
[62] V. G. Snider, B. J. Pella, A. Mukherjee, *Inorg. Chim. Acta* **2018**, *469*, 447–452.
[63] W. Kläui, W. Eberspach, P. Gütlich, *Inorg. Chem.* **1987**, *26*, 3977–3982.
[64] F. Ulatowski, K. Dabrowa, T. Balakier, J. Jurczak, *J. Org. Chem.* **2016**, *81*, 1746–1756.
[65] V. V. Pavlishchuk, A. W. Addison, *Inorg. Chem. Acta* **2000**, *298*, 97–102.
[66] A. Jaikumar, K. S. V. Santhanam, S. G. Kandlikar, I. B. P. Raya, P. Raghupathi, *ECS Trans.* **2015**, *66*, 55.
[67] A. L. Raithel, W. E. Meador, T.-Y. Kim, R. J. Staples, J. H. Delcamp, T. W. Hamann, *J. Am. Chem. Soc.* **2023**, *145*, 1367–1377.
[68] S. Aroua, T. K. Todorova, P. Hommes, L.-M. Chamoreau, H.-U. Reissig, V. Mougel, M. Fontecave, *Inorg. Chem.* **2017**, *56*, 5930–5940.
[69] P. Harding, D. J. Harding, R. Daengngern, T. Thurakitsaree, B. M. Schutte, M. J. Shaw, Y. Tantirungrotechai, *Polyhedron* **2012**, *42*, 291–301.
[70] B. P. Sullivan, D. J. Salmon, T. J. Meyer, J. Peedin, *Inorg. Chem.* **1979**, *18*, 3369–3374.
[71] P. Thordarson, "BindFit" can be found under http://supramolecular.org/ (accessed 16 December 2024).
[72] P. Thordarson, *Chem. Soc. Rev.* **2011**, *40*, 1305–1323.
[73] E. S. Böes, P. R. Livotto, H. Stassen, *Chem. Phys.* **2006**, *331*, 142–158.
[74] *CrysAlis*^{Pro}, version 1.171.37.35; Rigaku Oxford Diffraction (**2014**).
[75] G. M. Sheldrick, *Acta Crystallogr.* **2015**, *A71*, 3–8.
[76] G. M. Sheldrick, *Acta Crystallogr.* **2015**, *C71*, 3–8.
[77] Gaussian 09, Revision A.02, M. J. Frisch, G. W. Trucks, H. B. Schlegel, G. E. Scuseria, M. A. Robb, J. R. Cheeseman, G. Scalmani, V. Barone, G. A. Petersson, H. Nakatsuji, X. Li, M. Caricato, A. Marenich, J. Bloino, B. G. Janesko, R. Gomperts, B. Mennucci, H. P. Hratchian, J. V. Ortiz, A. F. Izmaylov, J. L. Sonnenberg, D. Williams-Young, F. Ding, F. Lipparini, F. Egidi, J. Goings, B. Peng, A. Petrone, T. Henderson, D. Ranasinghe, V. G. Zakrzewski, J. Gao, N. Rega, G. Zheng, W. Liang, M. Hada, M. Ehara, K. Toyota, R. Fukuda, J. Hasegawa, M. Ishida, T. Nakajima, Y. Honda, O. Kitao, H. Nakai, T. Vreven, K. Throssell, J. A. Montgomery, Jr., J. E. Peralta, F. Ogliaro, M. Bearpark, J. J. Heyd, E. Brothers, K. N. Kudin, V. N. Staroverov, T. Keith, R. Kobayashi, J. Normand, K. Raghavachari, A. Rendell, J. C. Burant, S. S. Iyengar, J. Tomasi, M. Cossi, J. M. Millam, M. Klene, C. Adamo, R. Cammi, J. W. Ochterski, R. L. Martin, K. Morokuma, O. Farkas, J. B. Foresman, and D. J. Fox, Gaussian, Inc., Wallingford CT, **2016**.
[78] A. D. Becke, *J. Chem. Phys.* **1993**, *98*, 5648–5652.
[79] C. Lee, W. Yang, R. G. Parr, *Phys. Rev.* **1998**, *37*, 785–789.
[80] T. H. Dunning III, P. J. Hay, In: H. F. Schaefer Jr., Editor, Methods of Electronic Structure Theory vol. 3, *Plenum Press* **1977**, 1–27.
[81] T. H. Dunning Jr., *J. Chem. Phys.* **1970**, *53*, 2823–2833.
[82] P. J. Hay and W. R. Wadt, *J. Chem. Phys.* **1985**, *82*, 284–398.
[83] P. J. Hay and W. R. Wadt, *J. Chem. Phys.* **1985**, *82*, 270–283.

Manuscript received: December 17, 2024
Revised manuscript received: February 13, 2025
Accepted manuscript online: February 14, 2025
Version of record online: February 25, 2025

© 2025 Wiley-VCH GmbH

10990682c, 2025, 11, Downloaded from https://chemistry-europe.onlinelibrary.wiley.com/doi/10.1002/ejic.202400835 by Universite Catholique De Louvain, Wiley Online Library on [06/06/2025]. See the Terms and Conditions (https://onlinelibrary.wiley.com/terms-and-conditions) on Wiley Online Library for rules of use; OA articles are governed by the applicable Creative Commons License